Nitric Oxide 89 (2019) 22–31

Contents lists available at ScienceDirect

Nitric Oxide

journal homepage: www.elsevier.com/locate/yniox

Reciprocal regulation of sulfite oxidation and nitrite reduction by mitochondrial sulfite oxidase

Alexander T. Kaczmarek[a,b], Marc J.F. Strampraad[c], Peter-Leon Hagedoorn[c], Guenter Schwarz[a,b,*]

[a] Institute of Biochemistry, Department of Chemistry, University of Cologne, Cologne, 50674, Germany
[b] Center for Molecular Medicine Cologne (CMMC), University of Cologne, Cologne, 50931, Germany
[c] Department of Biotechnology, Delft University of Technology, Van der Maasweg 9, 2629 HZ, Delft, the Netherlands

ARTICLE INFO

Keywords:
Sulfite oxidase
Molybdenum cofactor
Nitrate-nitrite-NO pathway
Nitrite reduction
Nitric oxide

ABSTRACT

The oxygen-independent nitrate-nitrite-nitric oxide (NO) pathway is considered as a substantial source of NO in mammals. Dietary nitrate/nitrite are distributed throughout the body and reduced to NO by the action of various enzymes. The intermembrane spaced (IMS), molybdenum cofactor-dependent sulfite oxidase (SO) was shown to catalyze such a nitrite reduction. In this study we asked whether the primary function of SO – sulfite oxidation – and its novel function – nitrite reduction – impact each other. First, we utilized benzyl viologen as artificial electron donor to investigate steady state NO synthesis by SO and found fast (k_{cat} = 14 s^{-1}) nitrite reduction of SO full-length and its isolated molybdenum domain at pH 6.5. Next, we determined the impact of nitrite on pre-steady state kinetics in SO catalysis and identified nitrite as a pH-dependent inhibitor of SO reductive and oxidative half reaction. Finally, we report on the time-dependent formation of the paramagnetic Mo(V) species following nitrite reduction and demonstrate that sulfite inhibits nitrite reduction. In conclusion, we propose a pH-dependent reciprocal regulation of sulfite oxidation and nitrite reduction by each substrate, thus facilitating quick responses to hypoxia induced changes in the IMS, which may function in protecting the cell from reactive oxygen species production.

1. Introduction

Since the discovery of nitric oxide (NO) as a gasotransmitter in 1987 [1], two major sources of NO have been described in mammals. First, the three tissue-specific NO synthases (NOS) – the neuronal, endothelial and inducible isoform – that catalyze the oxygen-dependent conversion of L-arginine to L-citrulline and NO [2] have been identified. Later, the oxygen-independent nitrate-nitrite-NO pathway, which involves nitrite reduction to NO by different families of proteins and enzymes, has been reported [3]. Growing evidence supports the hypothesis that NO derived from nitrate/nitrite has a substantial role in the protection against various diseases, like cardiovascular [4–7], metabolic [7–10], and respiratory diseases [11–13] as well as a key regulator of blood pressure [14–19] and flow [20–22], and endothelial function [18,23], ofttimes independent of the action of NOS synthases.

Nitrate is mainly derived from the diet – up to 80% from the consumption of vegetables [24] – and absorbed in the gut, where it is transported in to different tissues (like recently shown in the skeletal muscle [25]) or into the salivary glands [26,27]. In these glands dietary nitrate is highly concentrated and excreted via the salvia into the oral cavity, where nitrate is reduced to nitrite by the action of oral bacteria [28]. Swallowed nitrite is then either non-enzymatically reduced to NO due to acidic conditions in the stomach, which involves the protonation of nitrite followed by the release of NO [29], however, the rate of reduction is rather low. Alternatively, nitrite is reabsorbed in the gut and distributed throughout the body. Additionally to the reduction of nitrate, nitrite is also produced by oxidation of NO as well as taken up as dietary nitrite from vegetables, fruits or processed meats [24]. Under hypoxic conditions, potentially induced by ischemia or long-lasting exercise, nitrite is reduced to NO via the action of either heme-containing proteins such as hemo- [30], neuro- [31], myo- [32], and cytoglobin [33] and as recently described indoleamine 2,3-dioxygenase 1 (IDO1) [34] or by molybdenum cofactor (Moco)-dependent enzymes such as xanthine oxidoreductase (XOR) [35], aldehyde oxidase (AO) [36], mitochondrial amidoxime reducing component (mARC) [37] and sulfite oxidase (SO) [38].

Amongst the four Moco-dependent enzymes in humans, the cytosolic XOR was described first to reduce nitrite to NO and is by far the

* Corresponding author. Institute of Biochemistry, Department of Chemistry, University of Cologne, Cologne, 50674, Germany.
E-mail addresses: akaczmar@smail.uni-koeln.de (A.T. Kaczmarek), M.J.F.Strampraad@tudelft.nl (M.J.F. Strampraad), P.L.Hagedoorn@tudelft.nl (P.-L. Hagedoorn), gschwarz@uni-koeln.de (G. Schwarz).

https://doi.org/10.1016/j.niox.2019.04.004
Received 20 March 2019; Received in revised form 8 April 2019; Accepted 11 April 2019
Available online 17 April 2019

most extensively studied Moco enzyme in this regard, not only in vertebrates. Nitrite reduction takes place at the Moco using xanthine or NADH as electron donor and reduces nitrite to NO with a k_{cat} ranging from 0.33 s^{-1} to 2.32 s^{-1} and $K_M^{nitrite}$ = 3–4 mM [39]. The closely related AO exhibits nitrite reduction with similar enzymatic parameters (k_{cat} = 1.89 s^{-1}; K_M = 10 mM), which, also demonstrated for XOR, was reported to be oxygen sensitive and pH-dependent [39,40]. Recently, the outer mitochondrial membrane-localized mARC [41] was identified to also catalyze a nitrite reduction with k_{cat} = 0.1 s^{-1} and $K_M^{nitrite}$ = 9.5 mM [37]. Similar to XOR and AO, nitrite reduction was increased at a low pH and under hypoxic conditions. Computational analyses of two putative mechanisms, first an oxyl and second a hydroxyl radical transfer of mARC-dependent nitrite reduction were compared [42] and suggested the hydroxyl radical transfer as more favorable due to the involvement of a low pH-mediated protonation of nitrite to enable barrier-less one-electron transfer between Moco and nitrite. In the reaction of fully reduced Moco (Mo(IV)) with HNO_2, a paramagnetic Mo(V) species with an equatorial hydroxyl group is formed, which was confirmed by EPR studies of reduced mARC reacted with nitrite [42]. Interestingly, the resulting EPR spectra shared high similarities with the paramagnetic low-pH Mo(V) signal of SO, which was also described to harbor a equatorial hydroxyl group at Moco [43].

As the other mammalian Moco-dependent enzymes, SO was described to reduce nitrite to NO in a one-electron transfer reaction [38]. The homodimeric SO is localized in the intermembrane space (IMS) of mitochondria, where it catalyzes the oxidation of sulfite to sulfate, as the last step of the cysteine catabolism [44]. SO exhibits a three-domain structure, with an N-terminal heme domain, incorporating a cytochrome b_5-like heme cofactor, followed by a hinge region that continues to the Mo domain, incorporating the Moco and the C-terminal dimerization domain [45] (Fig. 1A). During sulfite oxidation, sulfite initiates a nucleophilic attack of its lone electron pair on the equatorial oxo group of Moco, which accepts two electrons causing the reduction of Mo(VI) to Mo(IV), termed as the reductive half reaction [46,47] (Fig. 1B). Following the release of sulfate from the active site, H_2O occupies the liberated equatorial Mo ligand position and the first intramolecular electron transfer (IET) between heme and Moco proceeds, termed as the oxidative half reaction, resulting in a SO with Fe(II) and Mo(V). Next, the physiological electron acceptor cytochrome *c* reoxidizes heme and a second IET forms the SO Fe(II)/Mo(VI) species. At last, a second cytochrome *c* fully reoxidizes SO into its resting state and the two SO-reduced cytochrome *c* molecules can fuel the respiratory chain [48].

Sulfite-reduced SO is able to use nitrite as an electron acceptor resulting in the formation of NO with a k_{et} = 0.0044 s^{-1} and $K_d^{nitrite}$ = 1.7 mM [38]. Interestingly, only the Mo(IV) species was found to reduce nitrite, arresting SO in a stable paramagnetic Mo(V) state in the absence of additional electron acceptors and therefore terminating catalysis following one turnover. However, by use of the one electron donor phenosafranine, steady state NO synthesis by SO was enabled with increased k_{cat} = 1.9 s^{-1} and K_M = 80 mM. Furthermore, comparison of SO wildtype (*wt*) with variants lacking the heme domain or the heme cofactor pointed towards a competition between nitrite and heme for the first electron, as well as steric hindrances caused by heme-Mo domain interactions [38]. Consistent with the other Moco-dependent enzymes, SO-dependent nitrite reduction was again increased with decreasing pH, which is in good agreement with subcellular localization of SO.

Although, nitrite-reduction by Moco-dependent enzymes is widely accepted as a major source of nitrite-derived NO [49], the underlying reaction mechanism is poorly understood. In this study we asked the question, how sulfite oxidation as the primary metabolic function in cysteine catabolism and the recently reported nitrite reduction impact each other. We hypothesize that sulfite regulates NO production of SO due to a competition of both substrates for the active site and propose the formation of a nitrito-O-Mo complex. Therefore, we investigated the reaction mechanism of sulfite-dependent nitrite reduction in SO by steady state kinetics and found a remarkably high k_{cat} = 14 s^{-1} when using benzyl viologen as electron donor. Pre-steady state kinetics of the oxidative and reductive half reaction in a nitrite-dependent manner as well as time-resolved EPR studies of the nitrite-dependent paramagnetic Mo(V) formation disclosed two orders of magnitude rate difference between sulfite oxidation and nitrite reduction. In aggregate, we confirmed the pH dependency of SO nitrite reduction and propose a reciprocal regulation of NO generation by sulfite and nitrite.

2. Materials and methods

2.1. Chemicals

Chemicals were purchased from Sigma-Aldrich if not stated otherwise. Sodium nitrite was acquired from Alfa Aesar.

2.2. Expression, and purification of recombinant proteins

His-tagged human SO was either expressed as the mature full-length enzyme (E80 – P545) or as the truncated Mo domain (A167 – P545) using pQE-80 L (Qiagen) based expression plasmids previously described [38]. Proteins were either expressed as the holo enzyme within the *E. coli* strain TP1004 [50] or as apo proteins within the Moco-deficient *E. coli* strain KB2066-*chlA3*$^-$ [51]. Expression was performed in 5 L Erlenmeyer flasks with 2 L cultures of LB-media, supplemented with 1 mM sodium molybdate and 250 µM IPTG for 72 h at 18 °C. Harvested cells were resuspended in lysis buffer (50 mM Tris/acetate pH 8.0, 250 mM NaCl, 10 mM imidazole) and lysed following the incubation with lysozyme (VWR; 23500 U/mg) for 30 min at room temperature and subsequent cell disruption utilizing the Emulsiflex C-5 cell disruptor (Avestin). Proteins were purified via Ni-NTA affinity chromatography using HIS-Select® Nickel Affinity Gel (Sigma-Aldrich) according to the manufactures protocol. Full-length SO was eluted with elution

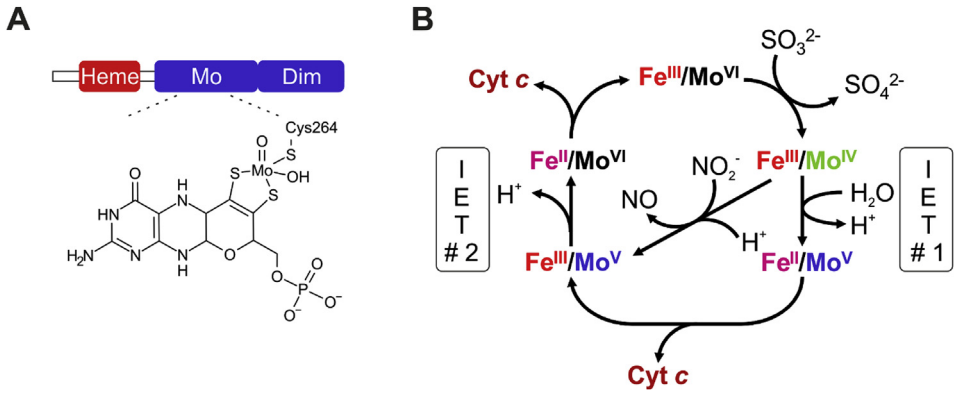

Fig. 1. Domain structure and catalytic cycle of human SO. (A) The three domains of SO function in cytochrome b_5-like heme binding (heme domain), Moco binding via Cys264 (Mo domain), and dimerization (Dim); (B) Reaction mechanism of sulfite oxidation and proposed nitrite reduction. The individual intermolecular electron transfer (IET) steps between Mo and heme Fe are depicted.

buffer (50 mM Tris/acetate pH 8.0, 250 mM NaCl, 250 mM imidazole) and buffer-exchanged into protein buffer (20 mM Tris/acetate pH 8.0, 50 mM NaCl). The His-tag of SO Mo domain (SO-Mo) was cleaved off on-column by incubation with the PreScission Protease (GE Healthcare) for 16 h at 4 °C. SO-Mo was further purified via anion exchange chromatography using a Source 15 Q column (GE healthcare, 15 mL) equilibrated with 50 mM Tris/Ac pH 8.0 and eluted with increasing concentrations of NaCl. Finally, SO-Mo was buffer-exchanged into protein buffer if not stated otherwise.

2.3. Determination of Moco saturation

Moco saturation of recombinantly expressed proteins was determined via the oxidation and dephosphorylation to dephospho-FormA and subsequent HPLC analysis as described [52]. Briefly, 100 pmol SO was oxidized with acidic lugol's iodine solution overnight and protected from light. After removal of precipitated protein, supernatant was treated with fresh 1% ascorbic acid and buffered with TRIS to pH 8.3. Dephosphorylation of phospho-FormA was acquired by alkaline phosphatase (Roche; 7500 U/ml) and addition of 20 mM $MgCl_2$, incubating for 30 min protected from light.

2.4. Steady state kineitcs

Steady state kinetics were conducted anaerobically and at RT in an anaerobic glove box (Coy laboratory products). Nitrite reduction by SO variants was measured by following absorption changes at 595 nm of semi-reduced benzyl viologen (BV^+) to oxidized BV^{2+} using a TECAN Sunrise™ plate reader (Tecan Austria). BV^{2+} was photochemically reduced to BV^+ via irradiation of a 2.5 mM BV^{2+} 100% isopropanol solution for 60 s with an UV lamp set to 350 nm (TL-900, CAMAG Berlin), as described previously [53]. SO variants were used in concentrations of 10 nM in reactions with varying concentrations of sodium nitrite and 400 µM BV^+. Initial slopes of observed reactions velocities were determined and subtracted from blank reactions lacking enzyme.

2.5. Pre-steady state kinetics

2.5.1. Stopped-flow spectroscopy

Pre-steady state kinetics were measured anaerobically at 10 °C using a SX20 stopped-flow spectrometer (Applied Photophysics Ltd.). Anaerobic preparation of the stopped-flow device, syringes, and tubings was achieved by oxygen scavenging via a mixture of 100 mM sodium acetate pH 5.0, 10 mM D-glucose, glucose oxidase (Sigma-Aldrich) and catalase (Sigma-Aldrich) for 1 h, followed by a washout with anaerobic assay buffer (50 mM Tris/acetate pH 8.0 or 50 mM Bis-Tris/acetate pH 6.5) [54]. Enzyme solutions were prepared anaerobically in a glove box (Coy laboratory products), by thawing in the box and buffer exchange into anaerobic assay buffer utilizing PD10 columns (GE Healthcare) according to the manufactures protocol. Reactions of 10 µM SO variants with sulfite or sulfite and nitrite with varying substrate concentrations where measured by either absorptions changes of the Moco at 414 nm when observing the Mo domain or absorption changes of the cytochrome b_5 heme at 423 nm when observing the mature full-length SO. Absorption changes were followed by a photon multiplier using a path length of 1 cm. Observed rate constants were determined by fitting single-, double-, or triple-exponential curves using an iterative non-linear least-squares Levenberg-Marquardt algorithm provided by the Pro-Data SX software.

2.5.2. EPR spectroscopy

EPR spectroscopy was conducted at a Bruker EMX spectrometer with liquid helium cooling as described [55]. Spectra were recorded with following EPR parameters: microwave frequency 9.4 GHz, microwave power 0.2 mW modulation frequency 100 kHz, modulation amplitude 1 Gauss, temperature 72 K. Over-modulated spectra were recorded at 10 Gauss modulation amplitude to increase signal-to-noise ratio for the low intensity samples. EPR signals of the Mo(V) spectrum were quantified by determination of the amplitude between the maxima at 3398 G and minima at 3410 G corresponding to the g_y signal. Resulting amplitudes were normalized against the time point with highest EPR signal. Sample preparation and reactions were conducted in an anaerobic glove box (Coy laboratory products) at RT. Enzyme solutions were made anaerobically by buffer exchange into anaerobic assay buffer (50 mM Bis-Tris pH 6.5) using a PD Minitrap G-25 column (GE Healthcare) according to the manufactures protocol. Either oxidized Mo domain was mixed with 1 mM sodium sulfite and 200 mM sodium nitrite, or sulfite-pre-reduced Mo domain was mixed with varying concentrations of sodium nitrite. Pre-reduced Mo domain was obtained by mixing enzyme with 1 mM sodium sulfite, followed by removal of excess substrate via buffer exchange into assay buffer. Reactions were initiated by mixing 100 µL of 50 µM Mo domain with 100 µL substrate in an EPR quartz tube and stopped by flash freezing in liquid-nitrogen-cooled isopentane (−160 °C).

2.6. Statistical analysis

Results were expressed as mean and standard deviation. Unpaired two-tailed students t-test were performed with a significance level of 95%. Statistical analyses were performed and graphs designed utilizing the statistical software GraphPad Prism version 5.00 for windows (GraphPad Software).

2.6.1. Determination of Michaelis-Menten kinetics

For the calculation of Michaelis-Menten kinetics of steady state reactions the initial velocity v_0 at varying substrate concentrations was fitted to a hyperbolic curve as shown below.

$$v_0 = (v_{max} * [S]) / (K_M + [S]) \quad (1)$$

With v_0 = initial velocity at [S], v_{max} = maximal velocity, [S] = substrate concentration, and K_M = Michaelis-constant.

The turnover number k_{cat} was calculated as shown below.

$$k_{cat} = v_{max} / [E_{total}] \quad (2)$$

with v_{max} = maximal velocity, $[E_{total}]$ = enzyme concentration.

2.6.2. Determination of pre-steady state kinetics

For the determination of pre-steady state constants k_{red} and K_d observed rate constants k_{obs} were fitted to a hyperbolic curve as shown below.

$$k_{obs} = (k_{red} * [S])/(K_d + [S]) \quad (3)$$

With k_{obs} = observed rate constant at [S], k_{red} = reduction rate constant, [S] = substrate concentration, and K_d = dissociation constant.

2.6.3. Determination of IC_{50} and K_i

For the determination of inhibition constants IC_{50} and K_i, residual activity was fitted to a sigmoidal curve as shown below.

$$Y = 100/(1 + 10\wedge((\log IC_{50} - [I])*H)) \quad (4)$$

With Y = normalized residual activity, IC_{50} = concentration of [I] where 50% of the activity is inhibited, [I] = inhibitor concentration, and H = Hill slope.

K_i was calculated as shown below.

$$IC_{50} = (1 + ([S]/K_M))*K_i \quad (5)$$

With IC_{50} = concentration of [I] where 50% of the activity is inhibited, [S] = substrate concentration, K_M = Michaelis-constant, and K_i = inhibition constant.

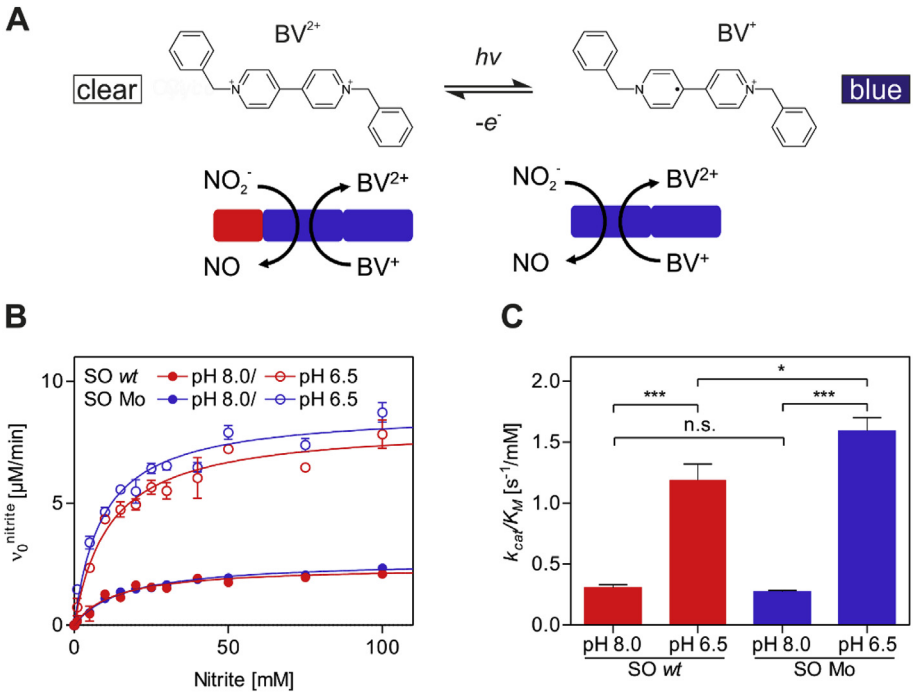

Fig. 2. Steady-state kinetics of nitrite reduction by SO using benzyl viologen (A) Photochemical reduction of oxidized benzyl viologen (BV^{2+}) to semi-reduced BV^{+} and scheme of catalyzed reactions by SO *wt* (left protein) and SO-Mo; (B) Michaelis-Menten kinetics and (C) Statistical analysis of kinetic efficiency of nitrite reduction by SO *wt* and SO-Mo at pH 8.0 and pH 6.5 (n = 3, n.s. = $p \geq 0.05$, * = $p \leq 0.05$, *** = $p \leq 0.001$).

3. Results

3.1. One electron donor benzyl viologen enables steady-state nitrite reduction by SO

Our previous studies showed different reaction velocities for sulfite- and phenosafranine-dependent SO nitrite reduction. Therefore, we searched for an alternative electron donor to further study nitrite reduction by SO. Bastian et al. described the use of semi-reduced benzyl viologen to reduce Moco of the bacterial Moco-dependent enzyme dimethyl sulfoxide reductase [56]. First, benzyl viologen was reduced by one equivalent of electrons to turn from the colorless BV^{2+} dication to the blue BV^{+} radical cation (Fig. 2A). An excess of BV^{+} radical cation was subsequently utilized to reduce the Moco of SO from Mo(VI) to Mo(IV). Upon addition of nitrite, BV-reduced SO *wt* as well as SO Mo domain (SO-Mo) was able to reduce nitrite to nitric oxide in a catalytic steady-state reaction as observed by the steady conversion of BV^{+} to BV^{2+} (Fig. 2B).

This finding goes beyond our previous single turn-over findings in nitrite reduction when using sulfite and demonstrates that NO synthesis by SO is not a dead end path of catalysis. Interestingly, nitrite reduction was strongly influenced by the pH; at pH 6.5 k_{cat} for both, SO *wt* and SO-Mo, was 3–4 fold increased, as compared to pH 8.0 (Table 1). Despite these differences, K_M values for all variants and pH conditions were in similar range of approx. 9–16 mM (Table 1). Furthermore, no difference in k_{cat} between full-length SO and SO-Mo domain was observed, suggesting that electrons provided by benzyl viologen were directly targeted to the catalytic Mo domain. However, at pH 6.5 but not at pH 8.0, kinetic efficiency k_{cat}/K_M was significantly lower for SO *wt* than SO-Mo (Fig. 2C). As control, measurements were also conducted with apo SO *wt* and apo SO-Mo variants lacking Moco (data not shown). Here, nitrite reduction or benzyl viologen oxidation was not observed, confirming previous findings that nitrite reduction requires Moco in SO.

Taken together, the benzyl viologen-dependent steady-state kinetics demonstrated the ability of SO to use an electron donor for catalytic reduction of nitrite to NO with similar k_{cat} values as observed for sulfite oxidation reaction when using the artificial electron acceptor ferricyanide [52] suggesting similar transition state barriers for catalysis. The increased $K_M^{nitrite}$ suggests a weaker binding of nitrite than sulfite to SO. In the past, when using sulfite as electron donor for nitrite reduction, dramatically lower k_{et} [37] values were reported, pointing towards a complex interplay of sulfite and nitrite within the SO active site. Therefore, pre-steady state kinetics of sulfite oxidation and the influence of nitrite were performed to provide additional insights into the underlying reaction mechanism.

Table 1
Kinetic parameters of SO catalyzed steady state nitrite reduction with benzyl viologen.

	SO *wt* pH 8.0	SO *wt* pH 6.5	SO-Mo pH 8.0	SO-Mo pH 6.5
k_{cat} [s^{-1}]	4.0 ± 0.1	13.7 ± 0.6	4.4 ± 0.1	14.7 ± 0.3
K_M [mM]	13.0 ± 1.5	11.5 ± 2.0	16.2 ± 0.9	9.2 ± 0.9

3.2. Nitrite inhibits the reductive half reaction of SO

Pre-steady state kinetics of the reductive half reaction were performed by UV/vis-spectroscopic measurements of changes in the absorption spectrum of SO-Mo utilizing stopped-flow analysis (Fig. 3A). SO-Mo lacking the strongly absorbing heme domain was reduced with sulfite causing Moco-specific absorption increase at 377 nm and decrease at 414 nm. We found a fast, sulfite-dependent Moco reduction with a k_{red}^{Mo} = 540.6 ± 25.4 s^{-1} and $K_d^{sulfite}$ = 89.8 ± 19.4 µM at pH 8.0 (Fig. 3B). Remarkably, reduction at pH 6.5 was even faster, and therefore Moco reduction was only measurable at low sulfite concentrations (20 µM), whereas at higher sulfite concentrations the reductive half reaction was completed already within the short mixing time of the sopped-flow device.

We then asked whether nitrite impacts this fast reductive half reaction and therefore monitored Moco reduction by 100 µM sulfite in the presence of different concentrations of nitrite at pH 8.0 (Fig. 3C). The reductive half reaction was inhibited with increasing concentrations of nitrite, with first inhibitory effects observed between 1 and 10 mM nitrite. With 100 µM sulfite present, sulfite oxidation was completely inhibited at concentrations of more than 560 mM nitrite resulting in an IC_{50} = 112.4 ± 58.1 mM and $K_i^{nitrite}$ = 53.1 ± 27.5 mM indicating that nitrite and sulfite both compete for the active site. The $K_i^{nitrite}$ is

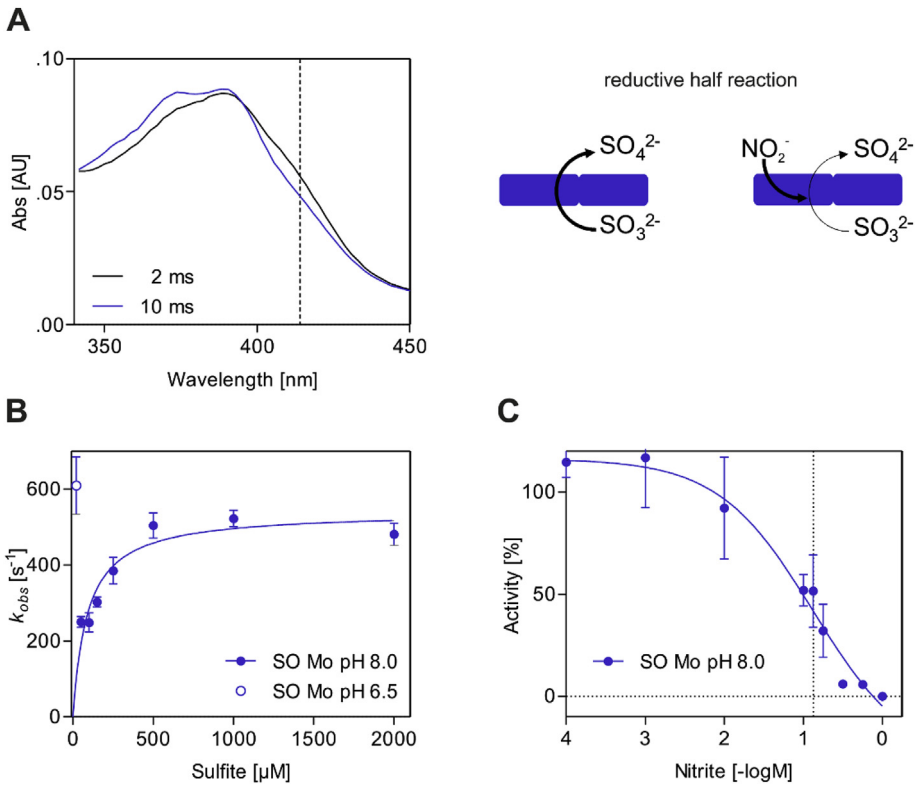

Fig. 3. Pre-steady-state kinetics of reductive half reaction and influence by nitrite. (A) Absorption changes of SO-Mo during reductive half reaction and scheme of SO-Mo catalyzed reductive half reaction with or without nitrite. (B) Pre-steady state kinetics of reductive half reaction and (C) its nitrite inhibition at pH 8.0 and pH 6.5.

consistent with the higher K_M for nitrite observed for benzyl viologen-dependent nitrite reduction and higher affinity of sulfite than nitrite for the active site of SO. Nitrite inhibition at pH 6.5 could be not determined due to the fact that the kinetic of the reductive half reaction at this pH was already completed within the mixing time of the stopped-flow device. Following the catalytic cycle, the next step is the oxidative half reaction, in which the first of the two sulfite-derived electrons is transferred to heme via the first IET step. Based on our results demonstrating nitrite-dependent inhibition of the reductive half reaction, the effect of nitrite on the oxidative half reaction was further investigated.

3.3. Heme competes with nitrite for the first sulfite-derived electron

Pre-steady state kinetics of the oxidative half-reaction were performed using UV/vis-spectroscopic measurements of SO *wt* heme reduction, monitored by the cytochrome b_5 Soret band shift from 413 to 423 nm (Fig. 4A). The rate of sulfite-dependent heme reduction was found to be one order of magnitude lower than the rate for Moco reduction, with $k_{red}^{heme} = 27.7 \pm 0.3\ s^{-1}$ and $K_d^{sulfite} = 7.7 \pm 0.5\ \mu M$ or $k_{red}^{heme} = 19.8 \pm 0.3\ s^{-1}$ and $K_d^{sulfite} = 2.2 \pm 0.2\ \mu M$ at pH 8.0 or pH 6.5, respectively (Fig. 4B). Contrary to the reductive half-reaction, the oxidative half reaction was 1.4 times faster at pH 8.0 as compared to pH 6.5, indicating a putative role of the protonation status of residues located on heme and/or Mo domain to enable interaction for efficient electron transfer between both domains. Interestingly, dissociation constants of the oxidative half reaction were significantly reduced compared to the reductive half reaction, identifying the IET from Moco to heme as the rate-limiting step.

Similar to the reductive half reaction, the first IET from Mo to heme was strongly influenced by the presence of nitrite (Fig. 4C). In the reaction of 100 µM sulfite with SO *wt*, increasing concentrations of nitrite inhibited heme reduction, resulting in an $IC_{50} = 173.1 \pm 13.8$ mM and $K_i^{nitrite} = 12.3 \pm 1.0$ mM or $IC_{50} = 45.0 \pm 0.6$ mM and $K_i^{nitrite} = 0.98 \pm 0.01$ mM, at pH 8.0 or pH 6.5, respectively. Strikingly, the $K_i^{nitrite}$ for the oxidative half reaction showed also a strong pH dependency, as demonstrated by the 12-times higher $K_i^{nitrite}$ at pH 8.0 compared to pH 6.5. This significant difference suggests an increased affinity of nitrite for the active site under conditions of increased protonation. Furthermore, the curve shape of nitrite inhibition significantly changed when compared between pH 8.0 and pH 6.5; at pH 6.5 the slope of decreasing activity was much steeper with a Hill slope $H = 8.8 \pm 0.5$ compared to pH 8.0 with $H = 1.8 \pm 0.1$, pointing towards a pH-dependent switch of inhibition sensitivity. Comparing SO *wt* and SO-Mo the $K_i^{nitrite}$ at pH 8.0 of the reductive half reaction was 4-times higher than for the oxidative half reaction. Accordingly, nitrite competes with sulfite for the active site – in the reductive half reaction – as well as with heme for the first sulfite-derived electron – in the oxidative half reaction. Taken together, sulfite oxidation was strongly influenced by nitrite and efficient NO synthesis is presumably dependent on sustaining a complex order of subsequent reactions, in which sulfite enters the active site before nitrite, followed by the oxidation to sulfate, its removal from the active site, and at last occupation of either nitrite or water in the free equatorial position of the Mo center, to initiate nitrite or heme reduction, respectively.

3.4. Sulfite inhibits nitrite reduction

In our study so far, sulfite oxidation parameters and the influence of nitrite on these were investigated. Therefore, the formation of a nitrite reduction-induced paramagnetic Mo(V) species in SO-Mo was investigated in a kinetic manner utilizing EPR spectroscopy (Fig. 5A). SO-Mo was mixed with 1 mM sulfite and 200 mM nitrite in a pH 6.5 buffer under anaerobic conditions and reactions were stopped at different time points by flash freezing mixtures in liquid nitrogen-cooled isopentane (−160 °C). Recorded EPR spectra resembled the well described low pH Mo(V) EPR signal with a visible ^1H hyperfine splitting at g_z, as described [43], with g-factor values of $g_{zyx} = 2.001, 1.973, 1.962$.

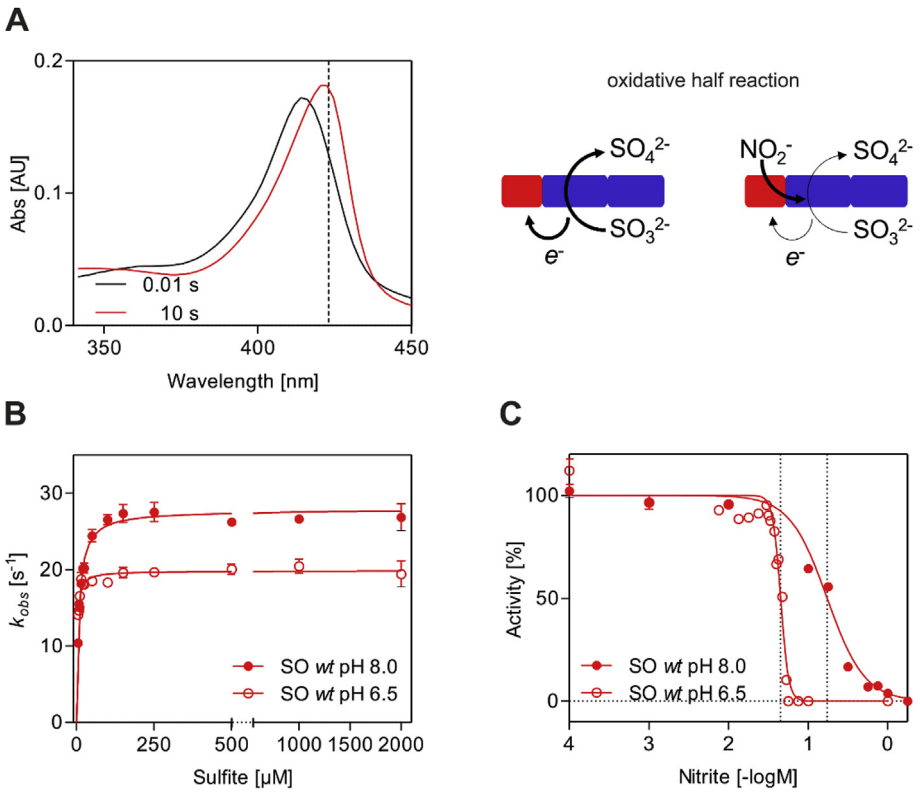

Fig. 4. Pre-steady-state kinetics of oxidative half reaction and influence by nitrite. (A) Absorption changes of SO *wt* during oxidative half reaction and scheme of SO *wt* catalyzed oxidative half reaction with or without nitrite. (B) Pre-steady state kinetics of oxidative half reaction and (C) its nitrite inhibition at pH 8.0 and pH 6.5.

Features of the EPR spectrum indicated the formation of Mo(V) with an equatorial hydroxyl group. With increasing time, the nitrite-dependent Mo(V) signal amplitude steadily increased and reached a plateau after approx. 70 s (Fig. 5B). Data distribution allowed a one-phase exponential fit with resulting k_{obs} = 0.08 ± 0.01 s^{-1}. Remarkably, the observed rate constant was three or four orders of magnitude lower than the oxidative or reductive half reaction following sulfite oxidation, respectively. Thus, slow observed Mo(V) formation again suggests a competition of sulfite with nitrite for the active site. Based on these observations, experiments without competing sulfite were conducted to determine rate constants for nitrite reduction-induced Mo(V) formation in the absence of sulfite competition.

Similar to the previous EPR measurements, SO-Mo was mixed with 200 mM nitrite and reactions were stopped via flash-freezing. To exclude sulfite as the competing element, SO-Mo was pre-reduced with 1 mM sulfite and excess sulfite (as well as produced sulfate) was removed via buffer exchange. EPR spectra of pre-reduced SO-Mo after reduction of nitrite resembled the same low pH Mo(V) signal as measured for the prior experiment (Fig. S1). Mo(V) formation was four times faster without excess sulfite, resulting in a k_{obs} = 0.34 ± 0.04 s^{-1} (Fig. 5B). Although, the rate of nitrite reduction had increased in absence of sulfite, the observed reaction rate remained nearly two orders of magnitude lower than the k_{cat} for benzyl viologen-dependent steady state nitrite reduction by SO.

4. Discussion

The primary metabolic function of SO is the catalysis of the final step of cysteine catabolism – the oxidation of sulfite to sulfate [44]. Since the discovery of SO's moon lightning function – the reduction of nitrite to NO – the impact of these two functions on each other remained elusive [38]. Our study contributed to a molecular understanding of the nitrite reductase function of SO and its pH-dependent reciprocal regulation by sulfite and nitrite. This reciprocal regulation has been demonstrated in three ways. First, we report a steady state nitrite reduction by SO using reduced benzyl viologen as electron

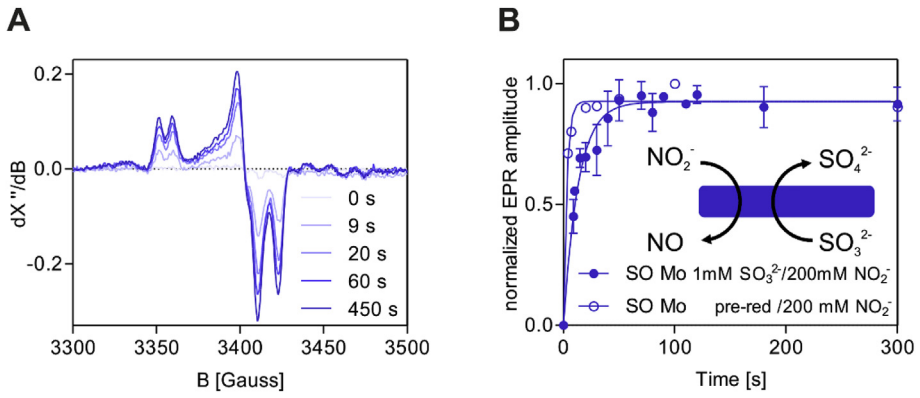

Fig. 5. Pre-steady state kinetics of SO-Mo nitrite reduction. (A) Nitrite-dependent Mo(V) EPR signal formation over time of SO-Mo reacted with 1 mM sulfite and 200 mM nitrite; (B) Pre-steady state kinetics of SO-Mo EPR signal of reactions with either 1 mM sulfite and 200 mM nitrite, or pre-reduced SO-Mo with 200 mM nitrite.

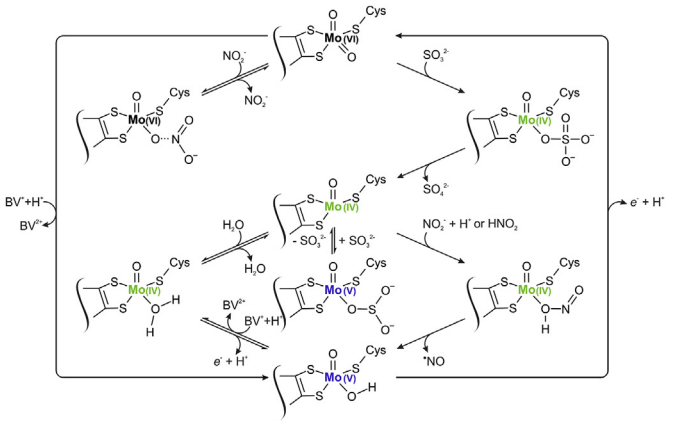

Fig. 6. Proposed catalytic cycle of SO catalyzed sulfite oxidation and nitrite reduction under conditions investigated in this study. BV = benzyl viologen.

donor. Second, we characterized the reductive and oxidative half reaction of SO and found a competing impact of nitrite on both reactions. Third, we analyzed time-dependent Mo(V) species formation following nitrite reduction. Consistent with the study of Wang et al., we confirmed pH-dependent nitrite reduction [38]. For mARC, another Moco-dependent nitrite reductase, Yang et al. have suggested that a hydroxyl radical transfer might occur, involving the formation of a nitrito-O-Mo complex and the protonation of the complexed Oα atom [42]. This hydroxyl reaction results in the formation of a paramagnetic Mo(V)-OH species, with an observable proton hyperfine splitting, a feature that we also found in our SO-Mo(V) EPR species.

When utilizing benzyl viologen as an electron donor, steady state nitrite reduction by SO was achieved and our determined k_{cat} (of SO *wt* at pH 8.0) was almost 7000 times higher as compared to reported k_{et} of NO release (SO *wt* at pH 7.4) with sulfite and 7 times faster than the k_{cat} reported for phenosafranine as electron donor [38]. In contrast to sulfite, benzyl viologen acts as a one-electron donor, thus after reduction of nitrite to NO and oxidation of Mo(IV) to Mo(V), benzyl viologen is able to re-reduce SO to Mo(IV). As reported, this Mo(IV) state is crucial for nitrite reduction as SO-Mo(V) is inert to nitrite [38]. Therefore, re-reduction by benzyl viologen enables characterization of steady state nitrite reduction by SO without sulfite. Absence of sulfite lead to a dramatic increase in nitrite reduction rate in comparison to previous findings, as nitrite can freely enter and NO leave the active site. Interestingly, at low pH, nitrite reduction was strongly increased pointing towards a required protonation of nitrite that enables a hydroxyl radical transfer reaction as proposed for mARC, another Moco-dependent nitrite reductase [42].

In addition to benzyl viologen steady state kinetics, we demonstrate a pH-dependent nitrite inhibition of sulfite oxidation by SO. The reductive as well as oxidative half reaction of sulfite oxidation were shown to be fully inhibited with increasing concentrations of nitrite. Noteworthy, we demonstrated that the resulting $K_i^{nitrite}$ for the reductive and oxidative half reaction where decreased at low pH, indicating an increased affinity of nitrite for the active site of SO. Whether this increased affinity is due to a protonation of nitrite to nitrous acid or rather due to changes of the protonation status within the SO active site, remains unclear. The reported pK_a of nitrous acid at 25 °C is 3.16 [57] and following a reformulation of the Henderson-Hasselbalch Equation (Eq. (6)),

$$K_a = ([H^+][A^-])/[HA] \quad (6)$$

with K_a = acid constant, [H+] = proton concentration, [A-] = conjugate base concentration, the [HA] = acid concentration can be calculated. Accordingly, at pH 6.5 nitrite is predominantly present with a ratio of approx. $2.2*10^3$:1 [NO_2^-]:[HNO_2] and at pH 8.0 with approx. $7*10^4$:1 [NO_2^-]:[HNO_2]. Therefore, nitrous acid concentration at pH 6.5 is 35 times higher compared to pH 8.0, which could at least partially accommodate for the 12 times higher $K_i^{nitrite}$ of the oxidative half reaction at pH 8.0 compared to pH 6.5. On the protein site, the hydroxyl group of residue Tyr343 was reported to facilitate substrate binding (Tyr322 in chicken SO crystal structure) [45] and to be important for oxidation of sulfite [58]. With its close proximity to the substrate binding site, Tyr343 could be a potential candidate for promoting nitrite protonation within the active site. Contrary, the high pK_a of 10.46 for isolated tyrosine would not suggest deprotonation of the hydroxyl group at changes from pH 6.5 to pH 8.0 that would explain the observed pH-dependent differences. However, in a folded protein surrounding residues may affect pK_a values dramatically as reported for a tyrosine pK_a in the active site of ketosteroid isomerase that was decreased to 6.3 [59]. Noteworthy, Tyr343 was shown to provide the substrate coordinating hydroxyl group in SO up to pH 10, as the Tyr343F mutant resulted in a dramatically increased $K_M^{sulfite}$ and $K_d^{sulfite}$ [58], which argues against lowered pK_a for Tyr343.

Our study suggests nitrite and sulfite competition for the active site, as demonstrated by the inhibition of the reductive half reaction by nitrite as well as inhibition of nitrite-dependent Mo(V) species formation by sulfite. In addition, we showed a nitrite competition with the heme cofactor for the Mo(IV) electron, as demonstrated by the inhibition of the oxidative half reaction. Strikingly, we found this reciprocal regulation of sulfite oxidation and nitrite reduction to be also pH-dependent. At pH 6.5 the Hill slope of nitrite-dependent inhibition was approx. five-fold higher as compared to pH 8.0, indicating a sensitivity switch of SO. As reviewed by Ferrel and Ha, Goldbeter and Koshland defined an input-output response as ultrasensitive when the ratio of IC_{90}/IC_{10} is smaller than 81 and sensitivity increases with decreasing ratio [60,61]. According to that, both measured inhibition curves for oxidative half reaction with $IC_{90}/IC_{10}{}^{pH8.0} = 11.5$ and $IC_{90}/IC_{10}{}^{pH6.5} = 1.6$ are classified as ultrasensitive, whereas the drop of pH dramatically increased the sensitivity. This switch in sensitivity could act as a response to acidifying conditions, as expected for the mitochondrial IMS, and primes SO to reduce nitrite to NO.

Based on our findings we propose a model integrating SO catalyzed sulfite oxidation as well as nitrite reduction, and elucidate the reciprocal regulation of both reactions by either substrate (Fig. 6). According to this model, SO in the resting state with Mo(VI) reacts with sulfite to form sulfate coordinated to a Mo(IV) species, with extremely fast k_{red} and low K_d. On the other hand, with increasing concentrations, nitrite enters the active site and blocks sulfite oxidation, which was demonstrated by the inhibition of the reductive half reaction. Next, sulfate leaves the active site and liberates the equatorial position. From here, the reaction might proceed via three routes. First, H_2O binds to Mo(IV) and the oxidative half reaction is initiated. Second, a new sulfite molecule binds to Mo(V) blocking the active site, detectable by EPR spectroscopy as reported previously [62]. Third, either nitrite or nitrous acid binds at the free equatorial position, forming a nitrito-O-Mo complex, similar to the proposal for mARC [42]. If nitrite binds to Mo (IV), protonation of the Oα is required to enable a barrier-less electron transfer [42]. Following release of NO from the active site, SO is present in a Mo(V)-OH state, exhibiting an EPR sensitive proton hyperfine splitting. To close the catalytic cycle, the second electron can be transferred via an intramolecular electron transfer to heme. In the benzyl viologen-dependent reaction, SO starts again in the resting state of Mo(VI). BV^+ donates presumably one electron to the equatorial oxo ligand of Moco, followed by a protonation, to end in Mo(V)-OH. Next, a second equivalent of BV^+ and a second H^+ fully reduce SO-Moco to Mo (IV), enabling the reduction of nitrite to NO. Similarly as described before, after NO release SO exhibits the Mo(V)-OH state. Again, BV^+ and one H^+ re-reduce SO to Mo(IV) to enable the steady state nitrite reduction by SO.

Besides NO, in the past years hydrogen sulfide (H_2S) was recognized as another gasotransmitter facilitating similar signal transductions as NO including blood pressure regulation [63]. One mechanism of H_2S

signaling is the persulfidation of free protein-thiols [44]. Prominent H_2S producers in mammals are cystathionine gamma-lyase (CSE), cystathionine beta synthase (CBS) and 3-mercaptopyruvate sulfurtransferase (MPST), which all generate H_2S during the non-oxidative catabolism of cysteine with the final product being sulfite [44]. Growing evidence demonstrates that H_2S and NO signaling reciprocally influence their respective signaling pathways [64,65]. Thus, it is quite astonishing that the catabolic end products of both gasotransmitters NO and H_2S are nitrite and sulfite, respectively.

The potential critical role of SO in NO signaling is further underlined by its localization in the IMS of mitochondria [66]. Due to its function in oxidative phosphorylation, the IMS and especially the outside of inner mitochondria membrane were reported to exhibit lowered pH of pH 6.8–6.5 [67,68], providing conditions optimal for SO-dependent nitrite reduction. Additionally, various targets of NO are located within mitochondria, the most prominent being complexes I, III and IV of the respiratory chain [69–72], thus SO derived NO is produced close to the point of action. At last, nitrite and NO were reported to exhibit cytoprotective effects during hypoxic events, caused by ischemia or long-lasting exercise [73]. Accordingly, under hypoxic conditions and low pH in the IMS, SO is expected to switch to its nitrite reductase function to deliver cytoprotective NO. Noteworthy, in the normal catalytic cycle of SO, cytochrome *c* reoxidizes the heme cofactor of SO. However, during hypoxia, the cytochrome *c* pool switches to a fully reduced state as the electron transfer to complex IV is arrested, thus increasing the likelihood for nitrite to accept the first electron from Mo(IV).

In recent years many studies provided strong evidence of beneficial effects for dietary nitrate/nitrite intake [6,24,74]. In our study, we demonstrated that the Moco-dependent SO might be a key nitrite reductase. Nitrite reduction by SO is reciprocally regulated by sulfite and nitrite in a pH-dependent manner, thus ensuring fast response to hypoxic conditions and ultimately to protect cells from reperfusion-induced oxidative stress. The localization of SO within the IMS identifies SO as a potential major producer of nitrite-derived NO in mitochondria and underlies its significance it may have as a NOS- and oxygen-independent NO source.

Conflicts of interest

The authors declare no conflict of interest.

Author contributions

Conceptualization, Alexander Tobias Kaczmarek and Guenter Schwarz; Data curation, Alexander Tobias Kaczmarek; Formal analysis, Alexander Tobias Kaczmarek and Peter-Leon Hagedoorn; Investigation, Alexander Tobias Kaczmarek, Marc J. F. Strampraad and Peter-Leon Hagedoorn; Visualization, Alexander Tobias Kaczmarek; Writing – original draft, Alexander Tobias Kaczmarek; Writing – review & editing, Alexander Tobias Kaczmarek, Peter-Leon Hagedoorn and Guenter Schwarz. All authors read and approved the final manuscript.

Funding

This research was funded by grant CMMC2017-C13 from the Center for Molecular Medicine Cologne, Germany. P.L.H acknowledges funding by grant NWO–CW 711.014.006 from the Council for Chemical Sciences of The Netherlands Organization for Scientific Research.

Acknowledgments

We thank Monika Laurien, Simona Jansen and Joana Stegemann for excellent technical assistance.

Appendix A. Supplementary data

Supplementary data to this article can be found online at https://doi.org/10.1016/j.niox.2019.04.004.

References

[1] L.J. Ignarro, R.E. Byrns, G.M. Buga, K.S. Wood, Endothelium-derived relaxing factor from pulmonary artery and vein possesses pharmacologic and chemical properties identical to those of nitric oxide radical, Circ. Res. (1987), https://doi.org/10.1161/01.RES.61.6.866.

[2] W.K. Alderton, C.E. Cooper, R.G. Knowles, Nitric oxide synthases: structure, function and inhibition, Biochem. J. 357 (2001) 593–615.

[3] A.W. DeMartino, D.B. Kim-Shapiro, R.P. Patel, M.T. Gladwin, Nitrite and nitrate chemical biology and signalling, Br. J. Pharmacol. 176 (2019) 228–245, https://doi.org/10.1111/bph.14484.

[4] S. Lidder, A.J. Webb, Vascular effects of dietary nitrate (as found in green leafy vegetables and beetroot) via the nitrate-nitrite-nitric oxide pathway, Br. J. Clin. Pharmacol. (2013), https://doi.org/10.1111/j.1365-2125.2012.04420.x.

[5] V. Kapil, E. Weitzberg, J.O. Lundberg, A. Ahluwalia, Clinical evidence demonstrating the utility of inorganic nitrate in cardiovascular health, Nitric Oxide -, Biol. Chem. (2014), https://doi.org/10.1016/j.niox.2014.03.162.

[6] S.A. Omar, A.J. Webb, Nitrite reduction and cardiovascular protection, J. Mol. Cell. Cardiol. (2014), https://doi.org/10.1016/j.yjmcc.2014.01.012.

[7] S.A. Omar, A.J. Webb, J.O. Lundberg, E. Weitzberg, Therapeutic effects of inorganic nitrate and nitrite in cardiovascular and metabolic diseases, J. Intern. Med. (2016), https://doi.org/10.1111/joim.12441.

[8] F.J. Larsen, J.O. Lundberg, M. Hezel, E. Weitzberg, M. Carlström, S. Borniquel, T. Nyström, Dietary inorganic nitrate reverses features of metabolic syndrome in endothelial nitric oxide synthase-deficient mice, Proc. Natl. Acad. Sci. Unit. States Am. (2010), https://doi.org/10.1073/pnas.1008872107.

[9] Z. Bahadoran, A. Ghasemi, P. Mirmiran, F. Azizi, F. Hadaegh, Beneficial effects of inorganic nitrate/nitrite in type 2 diabetes and its complications, Nutr. Metab. (2015), https://doi.org/10.1186/s12986-015-0013-6.

[10] L.D. Roberts, T. Ashmore, A.O. Kotwica, S.A. Murfitt, B.O. Fernandez, M. Feelisch, A.J. Murray, J.L. Griffin, Inorganic nitrate promotes the browning of white adipose tissue through the nitrate-nitrite-nitric oxide pathway, Diabetes (2015), https://doi.org/10.2337/db14-0496.

[11] V. Rihák, P. Zatloukal, J. Chládková, A. Zimulová, Z. Havlínová, J. Chládek, Nitrite in exhaled breath condensate as a marker of nitrossative stress in the airways of patients with asthma, COPD, and idiopathic pulmonary fibrosis, J. Clin. Lab. Anal. (2010), https://doi.org/10.1002/jcla.20408.

[12] R. Nadif, M. Rava, B. Decoster, H. Huyvaert, N. Le Moual, J. Bousquet, V. Siroux, R. Varraso, I. Pin, F. Zerimech, R. Matran, Exhaled nitric oxide, nitrite/nitrate levels, allergy, rhinitisand asthma in the EGEA study, Eur. Respir. J. (2014), https://doi.org/10.1183/09031936.00202413.

[13] M. Behnia, C.M. Wheatley, A. Avolio, B.D. Johnson, Influence of dietary nitrate supplementation on lung function and exercise gas exchange in COPD patients, Nitric Oxide 76 (2018) 53–61, https://doi.org/10.1016/J.NIOX.2018.03.009.

[14] A.J. Webb, N. Patel, S. Loukogeorgakis, M. Okorie, Z. Aboud, S. Misra, R. Rashid, P. Miall, J. Deanfield, N. Benjamin, R. MacAllister, A.J. Hobbs, A. Ahluwalia, Acute blood pressure lowering, vasoprotective, and antiplatelet properties of dietary nitrate via bioconversion to nitrite, Hypertension (2008), https://doi.org/10.1161/HYPERTENSIONAHA.107.103523.

[15] J. Petersson, M. Carlström, O. Schreiber, M. Phillipson, G. Christoffersson, A. Jägare, S. Roos, E.Å. Jansson, A.E.G. Persson, J.O. Lundberg, L. Holm, Gastroprotective and blood pressure lowering effects of dietary nitrate are abolished by an antiseptic mouthwash, Free Radic. Biol. Med. (2009), https://doi.org/10.1016/j.freeradbiomed.2009.01.011.

[16] V. Kapil, A.B. Milsom, M. Okorie, S. Maleki-Toyserkani, F. Akram, F. Rehman, S. Arghandawi, V. Pearl, N. Benjamin, S. Loukogeorgakis, R. MacAllister, A.J. Hobbs, A.J. Webb, A. Ahluwalia, Inorganic Nitrate Supplementation Lowers Blood Pressure in Humans: Role for Nitrite-Derived No, Hypertension, (2010), https://doi.org/10.1161/HYPERTENSIONAHA.110.153536.

[17] M. Gilchrist, A.C. Shore, N. Benjamin, Inorganic nitrate and nitrite and control of blood pressure, Cardiovasc. Res. (2011), https://doi.org/10.1093/cvr/cvq309.

[18] M. Gilchrist, P.G. Winyard, K. Aizawa, C. Anning, A. Shore, N. Benjamin, Effect of dietary nitrate on blood pressure, endothelial function, and insulin sensitivity in type 2 diabetes, Free Radic. Biol. Med. (2013), https://doi.org/10.1016/j.freeradbiomed.2013.01.024.

[19] V. Kapil, S.M.A. Haydar, V. Pearl, J.O. Lundberg, E. Weitzberg, A. Ahluwalia, Physiological role for nitrate-reducing oral bacteria in blood pressure control, Free Radic. Biol. Med. 55 (2013) 93–100, https://doi.org/10.1016/j.freeradbiomed.2012.11.013.

[20] H. Björne, J. Petersson, M. Phillipson, E. Weitzberg, L. Holm, J.O. Lundberg, Nitrite in saliva increases gastric mucosal blood flow, J. Clin. Investig. (2004), https://doi.org/10.1172/JCI200419019.Introduction.

[21] J. Petersson, M. Phillipson, E.A. Jansson, A. Patzak, J.O. Lundberg, L. Holm, Dietary nitrate increases gastric mucosal blood flow and mucosal defense, AJP Gastrointest. Liver Physiol. (2006), https://doi.org/10.1152/ajpgi.00435.2006.

[22] T.D. Presley, A.R. Morgan, E. Bechtold, W. Clodfelter, R.W. Dove, J.M. Jennings, R.A. Kraft, S. Bruce King, P.J. Laurienti, W. Jack Rejeski, J.H. Burdette, D.B. Kim-Shapiro, G.D. Miller, Acute effect of a high nitrate diet on brain perfusion in older adults, Nitric Oxide - Biol. Chem. (2011), https://doi.org/10.1016/j.niox.2010.10.

002.
[23] D.A. Hobbs, T.W. George, J.A. Lovegrove, The effects of dietary nitrate on blood pressure and endothelial function: a review of human intervention studies, Nutr. Res. Rev. (2013), https://doi.org/10.1017/S0954422413000188.
[24] N.G. Hord, Y. Tang, N.S. Bryan, Food sources of nitrates and nitrites: the physiologic context for potential health benefits, Am. J. Clin. Nutr. (2009), https://doi.org/10.3945/ajcn.2008.27131.
[25] C.N. Gilliard, J.K. Lam, K.S. Cassel, J.W. Park, A.N. Schechter, B. Piknova, Effect of dietary nitrate levels on nitrate fluxes in rat skeletal muscle and liver, Nitric Oxide 75 (2018) 1–7, https://doi.org/10.1016/J.NIOX.2018.01.010.
[26] J.O. Lundberg, Nitrate transport in salivary glands with implications for NO homeostasis, Proc. Natl. Acad. Sci. Unit. States Am. (2012), https://doi.org/10.1073/pnas.1210412109.
[27] X.M. Qu, Z.F. Wu, B.X. Pang, L.Y. Jin, L.Z. Qin, S.L. Wang, From nitrate to nitric oxide: the role of salivary glands and oral bacteria, J. Dent. Res. (2016), https://doi.org/10.1177/0022034516673019.
[28] J.J. Doel, N. Benjamin, M.P. Hector, M. Rogers, R.P. Allaker, Evaluation of bacterial nitrate reduction in the human oral cavity, Eur. J. Oral Sci. (2005), https://doi.org/10.1111/j.1600-0722.2004.00184.x.
[29] J.O.N. Lundberg, E. Weitzberg, J.M. Lundberg, K. Alving, Intragastric nitric oxide production in humans: measurements in expelled air, Gut (1994), https://doi.org/10.1136/gut.35.11.1543.
[30] R. Grubina, Z. Huang, S. Shiva, M.S. Joshi, I. Azarov, S. Basu, L.A. Ringwood, A. Jiang, N. Hogg, D.B. Kim-Shapiro, M.T. Gladwin, Concerted nitric oxide formation and release from the simultaneous reactions of nitrite with deoxy- and oxyhemoglobin, J. Biol. Chem. (2007), https://doi.org/10.1074/jbc.M700546200.
[31] M. Tiso, J. Tejero, S. Basu, I. Azarov, X. Wang, V. Simplaceanu, S. Frizzell, T. Jayaraman, L. Geary, C. Shapiro, C. Ho, S. Shiva, D.B. Kim-Shapiro, M.T. Gladwin, Human neuroglobin functions as a redox-regulated nitrite reductase, J. Biol. Chem. 286 (2011) 18277–18289, https://doi.org/10.1074/jbc.M110.159541.
[32] M. Totzeck, U.B. Hendgen-Cotta, P. Luedike, M. Berenbrink, J.P. Klare, H.J. Steinhoff, D. Semmler, S. Shiva, D. Williams, A. Kipar, M.T. Gladwin, J. Schrader, M. Kelm, A.R. Cossins, T. Rassaf, Nitrite regulates hypoxic vasodilation via myoglobin-dependent nitric oxide generation, Circulation (2012), https://doi.org/10.1161/CIRCULATIONAHA.111.087155.
[33] H. Li, C. Hemann, T.M. Abdelghany, M.A. El-Mahdy, J.L. Zweier, Characterization of the mechanism and magnitude of cytoglobin-mediated nitrite reduction and nitric oxide generation under anaerobic conditions, J. Biol. Chem. (2012), https://doi.org/10.1074/jbc.M112.342378.
[34] Y.J. Lim, T.C. Foo, A.W.S. Yeung, X. Tu, Y. Ma, C.L. Hawkins, P.K. Witting, G.N.L. Jameson, A.C. Terentis, S.R. Thomas, Human indoleamine 2,3-dioxygenase 1 is an efficient mammalian nitrite reductase, Biochemistry 58 (2019) 974–986, https://doi.org/10.1021/acs.biochem.8b01231.
[35] T.M. Millar, C.R. Stevens, N. Benjamin, R. Eisenthal, R. Harrison, D.R. Blake, Xanthine oxidoreductase catalyses the reduction of nitrates and nitrite to nitric oxide under hypoxic conditions, FEBS Lett. (1998), https://doi.org/10.1016/S0014-5793(98)00430-X.
[36] H. Li, T.K. Kundu, J.L. Zweier, Characterization of the magnitude and mechanism of aldehyde oxidase-mediated nitric oxide production from nitrite, J. Biol. Chem. (2009), https://doi.org/10.1074/jbc.M109.019125.
[37] C.E. Sparacino-Watkins, J. Tejero, B. Sun, M.C. Gauthier, J. Thomas, V. Ragireddy, B. a. Merchan, J. Wang, I. Azarov, P. Basu, M.T. Gladwin, Nitrite reductase and nitric-oxide synthase activity of the mitochondrial molybdopterin enzymes mARC1 and mARC2, J. Biol. Chem. 289 (2014) 10345–10358, https://doi.org/10.1074/jbc.M114.555177.
[38] J. Wang, S. Krizowski, K. Fischer-Schrader, D. Niks, J. Tejero, C. Sparacino-Watkins, L. Wang, V. Ragireddy, S. Frizzell, E.E. Kelley, Y. Zhang, P. Basu, R. Hille, G. Schwarz, M.T. Gladwin, Sulfite oxidase catalyzes single-electron transfer at molybdenum domain to reduce nitrite to nitric oxide, Antioxidants Redox Signal. 00 (2014) 150127063122000 10.1089/ars.2013.5397.
[39] L.B. Maia, V. Pereira, L. Mira, J.J.G. Moura, Nitrite reductase activity of rat and human xanthine oxidase, xanthine dehydrogenase, and aldehyde oxidase: evaluation of their contribution to NO formation in vivo, Biochemistry 54 (2015) 685–710, https://doi.org/10.1021/bi500987w.
[40] N. Cantu-Medellin, E.E. Kelley, Xanthine oxidoreductase-catalyzed reduction of nitrite to nitric oxide: insights regarding where, when and how, Nitric Oxide - Biol. Chem. (2013), https://doi.org/10.1016/j.niox.2013.02.081.
[41] J.M. Klein, J.D. Busch, C. Potting, M.J. Baker, T. Langer, G. Schwarz, C. Pottings, M.J. Baker, T. Langers, G. Schwarz, The mitochondrial amidoxime-reducing component (mARC1) is a novel signal-anchored protein of the outer mitochondrial membrane, J. Biol. Chem. 287 (2012) 42795–42803, https://doi.org/10.1074/jbc.M112.419424.
[42] J. Yang, L.J. Giles, C. Ruppelt, R.R. Mendel, F. Bittner, M.L. Kirk, Oxyl and hydroxyl radical transfer in mitochondrial amidoxime reducing component-catalyzed nitrite reduction, J. Am. Chem. Soc. 137 (2015) 5276–5279, https://doi.org/10.1021/jacs.5b01112.
[43] M.T. Lamy, S. Gutteridge, R.C. Bray, Electron-paramagnetic-resonance parameters of molybdenum(V) in sulphite oxidase from chicken liver, Biochem. J. 185 (1980) 397–403, https://doi.org/10.1042/bj1850397.
[44] J.B. Kohl, A.-T. Mellis, G. Schwarz, Homeostatic impact of sulfite and hydrogen sulfide on cysteine catabolism, Br. J. Pharmacol. 176 (2019) 554–570, https://doi.org/10.1111/bph.14464.
[45] C. Kisker, H. Schindelin, A. Pacheco, W.A. Wehbi, R.M. Garrett, K.V. Rajagopalan, J.H. Enemark, D.C. Rees, Molecular basis of sulfite oxidase deficiency from the structure of sulfite oxidase, Cell 91 (1997) 973–983, https://doi.org/10.1016/S0092-8674(00)80488-2.
[46] R. Hille, J. Hall, P. Basu, The mononuclear molybdenum enzymes, Chem. Rev. 114 (2014) 3963–4038, https://doi.org/10.1021/cr400443z.
[47] U. Kappler, J.H. Enemark, Sulfite-oxidizing enzymes, JBIC J. Biol. Inorg. Chem. 20 (2015) 253–264, https://doi.org/10.1007/s00775-014-1197-3.
[48] H.J. Cohen, S. Betcher-Lange, D.L. Kessler, K.V. Rajagopalan, Hepatic sulfite oxidase. Congruency in mitochondria of prosthetic groups and activity, J. Biol. Chem. 247 (1972) 7759–7766.
[49] D. Bender, G. Schwarz, Nitrite-dependent nitric oxide synthesis by molybdenum enzymes, FEBS Lett. 592 (2018) 2126–2139, https://doi.org/10.1002/1873-3468.13089.
[50] T. Palmer, C.L. Santini, C. Iobbi-Nivol, D.J. Eaves, D.H. Boxer, G. Giordano, Involvement of the narJ and mob gene products in distinct steps in the biosynthesis of the molybdoenzyme nitrate reductase in Escherichia coli, Mol. Microbiol. (1996), https://doi.org/10.1111/j.1365-2958.1996.tb02525.x.
[51] P. Hänzelmann, G. Schwarz, R.R. Mendel, Functionality of alternative splice forms of the first enzymes involved in human molybdenum cofactor biosynthesis, J. Biol. Chem. 277 (2002) 18303–18312, https://doi.org/10.1074/jbc.M200947200.
[52] J.L. Johnson, B.E. Hainline, K.V. Rajagopalan, B.H. Arison, The pterin component of the molybdenum factor. Structural characterization of two fluorescent derivatives, J. Biol. Chem. 259 (1984) 5414–5422.
[53] H. Kamogawa, T. Masui, S. Amemiya, Organic solid photochromism by photoreduction mechanism: viologen embedded in solid polar aprotic polymer matrix, J. Polym. Sci. Polym. Chem. Ed. 22 (1984) 383–390, https://doi.org/10.1002/pol.1984.170220210.
[54] C.E. Aitken, R.A. Marshall, J.D. Puglisi, An oxygen scavenging system for improvement of dye stability in single-molecule fluorescence experiments, Biophys. J. 94 (2008) 1826, https://doi.org/10.1529/biophysj.107.117689.
[55] B. Srour, M.J.F. Strampraad, W.R. Hagen, P.-L. Hagedoorn, Refolding kinetics of cytochrome c studied with microsecond timescale continuous-flow UV–vis spectroscopy and rapid freeze-quench EPR, J. Inorg. Biochem. 184 (2018) 42–49, https://doi.org/10.1016/J.JINORGBIO.2018.04.011.
[56] N.R. Bastian, C.J. Kay, M.J. Barber, K.V. Rajagopalan, Spectroscopic studies of the molybdenum-containing dimethyl sulfoxide reductase from Rhodobacter sphaeroides f. sp. denitrificans, J. Biol. Chem. 266 (1991) 45–51.
[57] G. Da Silva, E.M. Kennedy, B.Z. Dlugogorski, Ab initio procedure for aqueous-phase pKa calculation: the acidity of nitrous acid, J. Phys. Chem. A (2006), https://doi.org/10.1021/jp0639243.
[58] H.L. Wilson, K.V. Rajagopalan, The role of tyrosine 343 in substrate binding and catalysis by human sulfite oxidase, J. Biol. Chem. 279 (2004) 15105–15113, https://doi.org/10.1074/jbc.M314288200.
[59] J.P. Schwans, F. Sunden, A. Gonzalez, Y. Tsai, D. Herschlag, Uncovering the determinants of a highly perturbed tyrosine pKa in the active site of ketosteroid isomerase, Biochemistry (2013), https://doi.org/10.1021/bi401083b.
[60] J.E. Ferrell, S.H. Ha, Ultrasensitivity part I: Michaelian responses and zero-order ultrasensitivity, Trends Biochem. Sci. (2014), https://doi.org/10.1016/j.tibs.2014.08.003.
[61] J.E. Ferrell, S.H. Ha, Ultrasensitivity part II: multisite phosphorylation, stoichiometric inhibitors, and positive feedback, Trends Biochem. Sci. (2014), https://doi.org/10.1016/j.tibs.2014.09.003.
[62] R.C. Bray, M.T. Lamy, S. Gutteridge, T. Wilkinson, Evidence from electron-paramagnetic-resonance spectroscopy for a complex of sulphite ions with the molybdenum centre of sulphite oxidase, Biochem. J. 201 (1982) 241–243, https://doi.org/10.1042/bj2010241.
[63] H. Van Goor, J.C. Van Den Born, J.L. Hillebrands, J.A. Joles, Hydrogen sulfide in hypertension, Curr. Opin. Nephrol. Hypertens. (2016), https://doi.org/10.1097/MNH.0000000000000206.
[64] A.L. King, D.J. Polhemus, S. Bhushan, H. Otsuka, K. Kondo, C.K. Nicholson, J.M. Bradley, K.N. Islam, J.W. Calvert, Y.-X. Tao, T.R. Dugas, E.E. Kelley, J.W. Elrod, P.L. Huang, R. Wang, D.J. Lefer, Hydrogen sulfide cytoprotective signaling is endothelial nitric oxide synthase-nitric oxide dependent, Proc. Natl. Acad. Sci. Unit. States Am. (2014), https://doi.org/10.1073/pnas.1321871111.
[65] D.J. Polhemus, D.J. Lefer, Emergence of hydrogen sulfide as an endogenous gaseous signaling molecule in cardiovascular disease, Circ. Res. (2014), https://doi.org/10.1161/CIRCRESAHA.114.300505.
[66] J.M. Klein, G. Schwarz, Cofactor-dependent maturation of mammalian sulfite oxidase links two mitochondrial import pathways, J. Cell Sci. 125 (2012) 4876–4885, https://doi.org/10.1242/jcs.110114.
[67] A.M. Porcelli, A. Ghelli, C. Zanna, P. Pinton, R. Rizzuto, M. Rugolo, pH difference across the outer mitochondrial membrane measured with a green fluorescent protein mutant, Biochem. Biophys. Res. Commun. 326 (2005) 799–804, https://doi.org/10.1016/j.bbrc.2004.11.105.
[68] B. Rieger, W. Junge, K.B. Busch, Lateral pH gradient between OXPHOS complex IV and F(0)F(1) ATP-synthase in folded mitochondrial membranes, Nat. Commun. (2014), https://doi.org/10.1038/ncomms4103.
[69] G.C. Brown, Regulation of mitochondrial respiration by nitric oxide inhibition of cytochrome c oxidase, Biochim. Biophys. Acta Bioenerg. (2001), https://doi.org/10.1016/S0005-2728(00)00238-3.
[70] G.C. Brown, V. Borutaite, Inhibition of mitochondrial respiratory complex I by nitric oxide, peroxynitrite and S-nitrosothiols, Biochim. Biophys. Acta Bioenerg. (2004), https://doi.org/10.1016/j.bbabio.2004.03.016.
[71] L.B. Valdez, D.E. Iglesias, S.S. Bombicino, A. Boveris, Biochemical characterization of mitochondrial complex III inhibition by nitric oxide, Free Radic. Biol. Med. 53 (2012) S188–S189, https://doi.org/10.1016/J.FREERADBIOMED.2012.08.396.
[72] P. Sarti, E. Forte, A. Giuffrè, D. Mastronicola, M.C. Magnifico, M. Arese, The chemical interplay between nitric oxide and mitochondrial cytochrome c oxidase:

reactions, effectors and pathophysiology, Int. J. Cell Biol. (2012), https://doi.org/10.1155/2012/571067.

[73] C.K. Pride, L. Mo, K. Quesnelle, R.K. Dagda, D. Murillo, L. Geary, C. Corey, R. Portella, S. Zharikov, C. St Croix, S. Maniar, C.T. Chu, N.K.H. Khoo, S. Shiva, Nitrite activates protein kinase A in normoxia to mediate mitochondrial fusion and tolerance to ischaemia/reperfusion, Cardiovasc. Res. 101 (2014) 57–68, https://doi.org/10.1093/cvr/cvt224.

[74] A. Dejam, C.J. Hunter, C. Tremonti, R.M. Pluta, Y.Y. Hon, G. Grimes, K. Partovi, M.M. Pelletier, E.H. Oldfield, R.O. Cannon, A.N. Schechter, M.T. Gladwin, Nitrite infusion in humans and nonhuman primates: endocrine effects, pharmacokinetics, and tolerance formation, Circulation (2007), https://doi.org/10.1161/CIRCULATIONAHA.107.712133.